

Numerical Analyses of a Piled Raft Foundation with Grid-Form DMWs under Large-Scale Earthquakes

格子状地盤改良を併用したパイルド・ラフト基礎のレベル2地震に対する解析的検討

Yoshimasa Shigeno 重野 喜政*¹ Junji Hamada 濱田 純次*²
Naohiro Nakamura 中村 尚弘*³ Kiyoshi Yamashita 山下 清*⁴

Summary

Nonlinear seismic response analyses are conducted to evaluate seismic performance of a piled raft foundation with grid-form deep mixing walls (DMWs) subjected to dynamic load during large-scale earthquakes. Based on the previous study on a 12-story building under the middle-scale earthquake, the seismic response analyses are carried out using a detailed 3D FE model with the nonlinear soil model in which both tensile and shear criteria for the stabilized soil are considered. Consequently, it was found that the grid-form DMWs are quite effective in reducing the sectional force of piles to an acceptable level, even if the induced stress in the DMWs partially fails during the large-scale earthquakes.

Keywords: piled raft foundation, grid-form DMWs, large-scale earthquake, soil and structure interaction analysis, performance based design

梗概

格子状地盤改良を併用したパイルド・ラフト基礎のレベル2入力地震動に対する耐震性能を解析的に検討した。軟弱地盤上の12階建て免震建物を対象とし、詳細な3次元建物・地盤連成系有限要素によりモデル化した。地盤には、ひずみ依存特性に基づく非線形モデルを用い、改良土には、引張強度とせん断強度を考慮した非線形モデルを用いた。このモデルの中地震に対する妥当性は、2011年東北地方太平洋沖地震の観測値により検証されている。レベル2入力地震動を用いた解析の結果、格子状改良体の一部に破壊が生じるが改良体の機能は保持され、杭の断面力は許容値以下になることがわかった。

キーワード：パイルド・ラフト基礎、格子状地盤改良、基礎免震、相互作用解析、性能設計

1 INTRODUCTION

The aim of this study is to evaluate seismic performance of a piled raft foundation with grid-form cement deep mixing walls (DMWs) subjected to dynamic load during large-scale earthquakes. As to the piled raft foundation in soft ground supporting a 12-story building, field monitoring on the foundation settlement and the load sharing between the piles and the raft has been performed both statically and dynamically, and the seismic response of the soil-foundation system was successfully recorded at the time of the 2011 off the Pacific Coast of Tohoku Earthquake. In previous studies, the seismic response analysis using a detailed three dimensional (3D) finite element (FE) model has been conducted under the input ground motion recorded during the 2011 off the Pacific Coast of Tohoku Earthquake. In the analysis, soil model with equivalent modulus was used since the ground motion was categorized in middle-scale earthquakes at the observation site. The analytical results agreed well with the observation records as reported by Onimaru et al. (2012) and Hamada et al. (2014). However, a nonlinear soil model is essential to investigate the response under large-scale earthquakes, so that the analytical study using nonlinear soil model against the same input ground motion has been also conducted (Shigeno, 2015).

*1 Chief Researcher, Research & Development Institute 技術研究所 主任研究員

*2 Chief Researcher, Research & Development Institute, Dr. Eng. 技術研究所 主任研究員 博士(工学)

*3 Group Leader, Research & Development Institute, Dr. Eng. 技術研究所 構造部 応用数理グループ長 博士(工学)

*4 Executive Manager, Research & Development Institute, Dr. Eng. 技術研究所 専門役 博士(工学)

Based on the studies on the soil and structure response under the middle-scale earthquake, the seismic response analyses of the piled raft foundation are conducted using a 3D FE model with the nonlinear soil model in which both tensile and shear criteria for the stabilized soil are considered, focusing on the sectional force of the piles surrounded by the grid-form DMWs.

2 BUILDING AND GROUND CONDITIONS

The building analyzed is a 12-story residential building located in Tokyo. The building is a reinforced concrete structure with a seismic base isolation system; it was completed in 2008. Figure 1 shows a schematic view of the building and its foundation with the soil profile. The soil profile down to a depth of 7 m is fill, soft silt and loose silty sand. Between the depths of 7 m and 44 m, the profile is very soft to medium silty clay. The ground water table appears approximately 1.8 m below the ground surface. The building is supported by a piled raft with grid-form DMWs which were employed to prevent liquefaction of the silty sand between depths of 3 and 7 m as well as to improve the bearing capacity of the raft foundation (Yamashita et al., 2011). Figure 2 shows the foundation plan with the locations of both static and seismic monitoring devices. The spacing between the DMWs was about 6 to 9 m and an area replacement ratio (ratio of area of walls to total plan area) was 25%. The design standard strength of the stabilized soil was 1.8 MPa. At the time of the 2011 off the Pacific Coast of Tohoku Earthquake, the seismic response of the soil-foundation system, i.e., axial force and bending moment of two piles, contact pressure and pore water pressure beneath the raft, and accelerations of the ground and structure, were successfully recorded (Yamashita et al., 2012; Hamada et al., 2012).

3 NUMERICAL ANALYSES

3.1 Finite element mesh

Figure 3 shows the finite element (FE) mesh. The number of elements is 213,622 and the number of degrees-of-freedom (DOF) is 656,543. The building is modeled by elastic bars and shells. The piles are also modeled by elastic bars. Table 1 shows the material properties of the piles.

Figure 4 shows the top view of the FE mesh beneath the raft. To consider the shape and volume of the piles, cavities in the shape of the piles are made in the FE model. The nodes of the piles and the adjacent ground nodes at the same depth are bound by rigid bar elements. The base isolation layer is modeled by tri-linear spring elements. The lateral boundaries are periodic boundaries. They are positioned at 60 m outside of the building to minimize the boundary effect. The bottom is a viscous boundary. The engineering bedrock is set at a depth of 75 m from the ground surface.

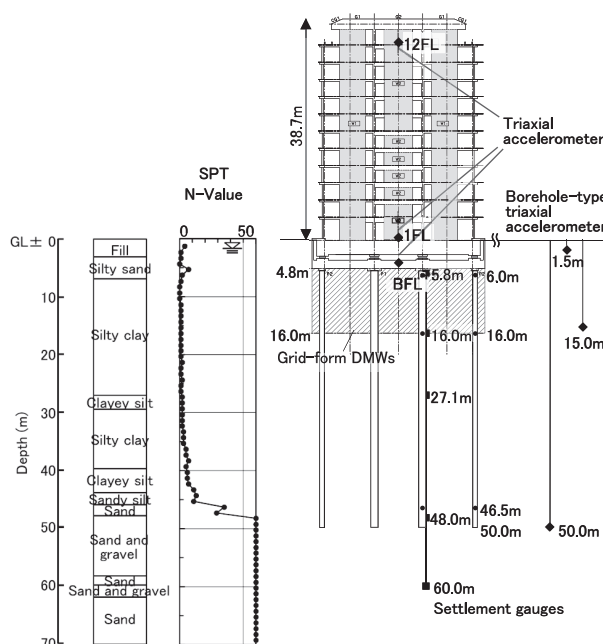


Fig. 1 Schematic view of building and foundation with soil profile

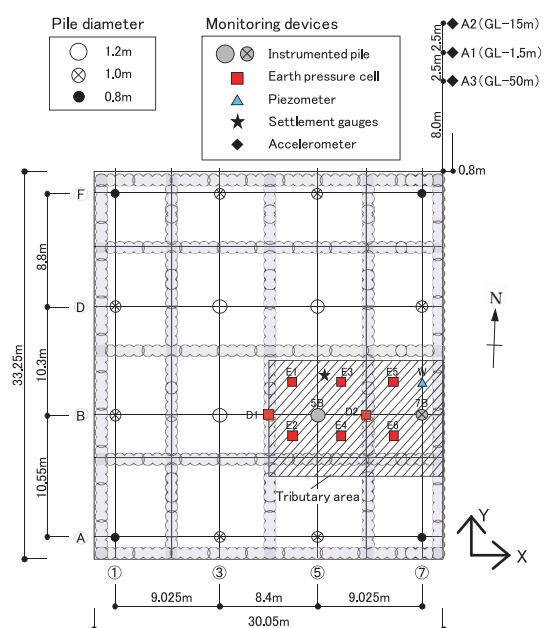


Fig. 2 Foundation plan with locations of monitoring devices

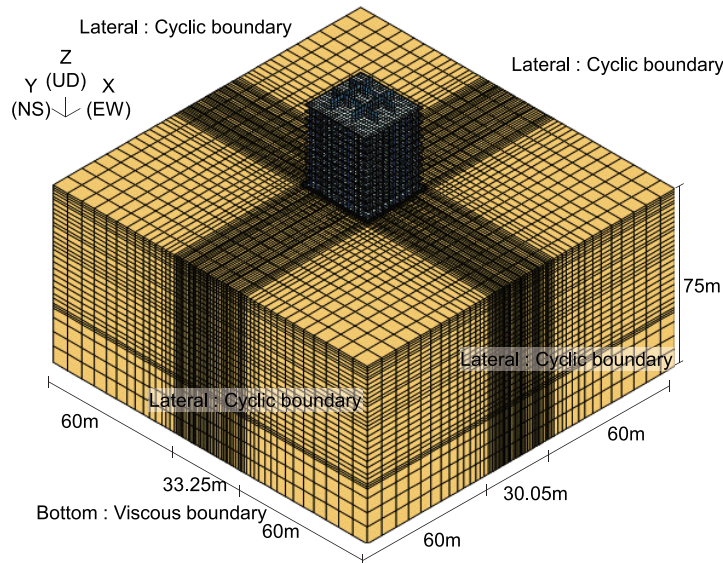


Fig. 3 FE mesh of the ground-structure interaction model

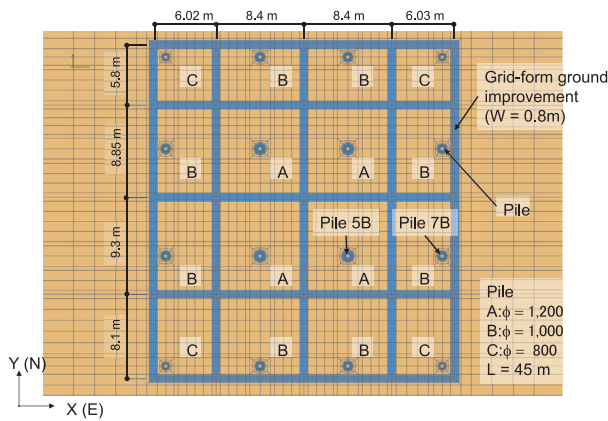


Fig. 4 Magnified plan view of FE mesh beneath the raft

Table 1 Material characteristics of piles

Pile diameter	(mm)	800	1000	1200
Young's modulus	(MN/m ²)	40000	40000	40000
Damping	(%)	2	2	2
Ae of SC pile	(m ²)	0.3268	0.4649	0.6714
Ie of SC pile	(m ⁴)	0.02199	0.04899	0.10316
Ae of PHC pile	(m ²)	0.2441	0.3633	0.5054
Ie of PHC pile	(m ⁴)	0.01455	0.03437	0.06958

Ae : Equivalent cross-sectional area
Ie : Equivalent moment of inertia of area

3.2 Input motions

In this paper, large scale earthquakes as maximum consideration earthquakes are defined by about 500 years recurrence interval. Two input ground motions were chosen from notification waves of Japan. Notification waves are generated using the acceleration response spectrum at engineering bedrock that is prescribed by Order for Enforcement of the Building Standards Act of Japan. The Kobe phase notification wave was used as an epicentral earthquake and the Hachinohe phase notification was used as a subduction zone earthquake. The input motions are denoted as Kobe phase and Hachinohe phase here after. Kobe phase was simulatively generated to fit the prescribed acceleration response spectrum using the phase characteristics recorded in Great Hanshin Earthquake (1995) at Kobe Marine Observatory. Hachinohe phase was generated the same way using the records in Tokachi - Oki Earthquake (1968) at Hachinohe Bay. In addition, Northern Tokyo Bay earthquake (denoted as Northern Tokyo Bay) that the Central Disaster Management Council of Japan was simulatively generated was also selected. Northern Tokyo Bay earthquake was simulated as an interplate earthquake whose epicenter is directly below the northern part of Tokyo Bay. This earthquake is assumed to cause the most severe damage to Tokyo metropolitan area.

Two directional input motions that are the EW wave and the NS wave are applied simultaneously. The time interval is 0.01 s and the analysis time is 120 s. Figure 5 shows the input accelerations in the EW and NS directions at the bedrock (the waves are 2E). Figure 6 shows the acceleration response spectrum of the input waves. Response spectrum of Kobe phase and Hachinohe phase is similar due to the generation method. But acceleration wave of Kobe phase has strong motion and rapid damping that are often seen in the epicentral earthquake. On the other hand, acceleration wave of Hachinohe phase has a feature of long time continuing large vibration that is often seen in the subduction zone earthquake. Northern Tokyo Bay has larger spectrum at the short period of less than 1.0 sec. But the spectrum becomes smaller than the other two waves during the period longer than 1.0 sec.

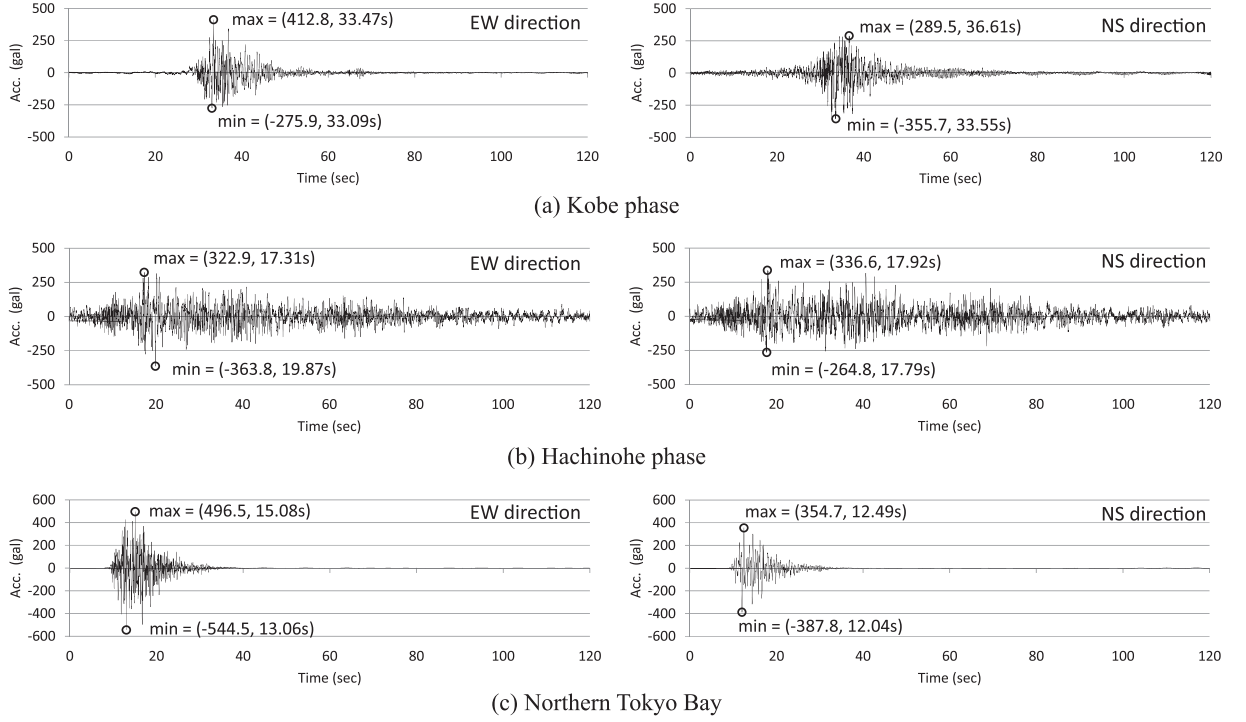


Fig. 5 Input accelerations at a depth of 75m (2E)

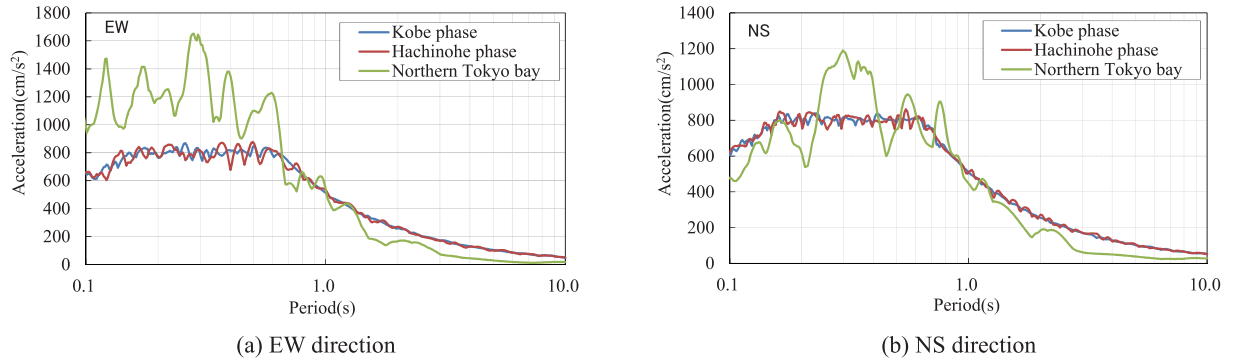


Fig. 6 Acceleration response spectrum of the input motion waves

The analysis code is an in-house program called MuDIAN developed by Shiomi et al. (1998). This code is parallelized by the hybrid parallel method and is able to calculate a large-DOF model with high speed as described in Shigeno et al. (2014).

3.3 Constitutive model of soil

A multi-hardening model proposed by Shiomi and Fujiwara (2014) is used as the constitutive model for the soil. This model is based on the multi-dimensional Yoshida model (Ishihara et al., 1985; Yoshida and Tsujino, 1993). The Yoshida model is characterized using G - γ and h - γ characteristics directly as input data. The Yoshida model uses a non-linear elastic model for the stress-strain relation. This causes overestimation of the strain under multi directional input-motion. A multi-hardening model uses an elasto-plastic model for the stress-strain relation. Therefore the direction of softening can be considered.

Nonlinearity before the stress reaches yield state is expressed by a hardening coefficient H' defined by equation (1). G_T is the tangential shear modulus that is evaluated from the τ - γ curve. The τ - γ curve under the simple shear condition is obtained from the G - γ characteristics.

$$H' = \frac{G_T}{1 - \frac{G_T}{G_0}} \quad (1)$$

The hardening coefficient H' appears in the denominator of the plastic multiplier $d\lambda$ derived as follow

$$d\lambda = \frac{\frac{\partial f^T}{\partial \sigma} \mathbf{D}_e d\epsilon}{H' + \frac{\partial f^T}{\partial \sigma} \mathbf{D}_e \frac{\partial f}{\partial \sigma}} \quad (2)$$

where \mathbf{D}_e is an elastic modulus tensor, and f is a yield function.

3.4 Soil properties

The shear wave velocity profile in the ground is obtained by an optimization method. The error in the transfer function is adapted as a cost function for the optimization. Observation records of small earthquakes that occurred before the 2011 off the Pacific Coast of Tohoku Earthquake were used in the optimization as target data (Onimaru et al., 2012). The P-S logging results are applied as the initial V_s distribution of the optimization. The initial shear modulus distribution for the analysis is created from the optimized V_s distribution. Figure 7 shows the distribution of the optimized V_s . The nonlinear characteristics of the ground were obtained from the cyclic triaxial tests of the samples. Figure 8 shows the G - γ and h - γ relations of each soil layer at this site.

The subloading Mohr-Coulomb model is used for the stress and strain relation of the multi-hardening model. The parameters related to shear strength are needed. The shear strength is given as cohesion. The cohesion of layers except for being investigated is assumed to follow equation (3).

$$c = G_0 \gamma_{50} \quad (3)$$

In this analysis, liquefaction is not considered though liquefaction may occur in the sand layer between depths of 3 and 7 m under large-scale earthquakes. Further research based on effective stress analysis is necessary to examine the effect of liquefaction on reduction of the soil shear modulus.

3.5 Constitutive model of stabilized soil

The DMWs are made from the mixture of cement milk and soil. The failure property is characterized by tensile strength, compressive strength and shear strength. The compressive strength of stabilized soil is very high and the failure due to the ground motion is caused by tensile or shear. Mohr-Coulomb yield criterion and Drucker-Prager yield criterion are often applied for the stabilized soil. These models give shear strength that depends on confining pressure. They are also able to give tensile strength if the friction angle is not zero. But the tensile strength of these models is larger than the real value in general. The tensile criterion has to be used to evaluate the correct tensile strength.

Maximum principal stress σ_1 that means the maximum tensile stress (note that tension is plus) is expressed using stress variants J'_2 and σ_m by applying Lode angle θ ($-\pi/6 < \theta < \pi/6$)

$$\sigma_1 = \frac{2(J'_2)^{1/2}}{\sqrt{3}} \sin\left(\theta + \frac{2\pi}{3}\right) + \sigma_m \quad (4)$$

where J'_2 is the second variant of deviatoric stress and σ_m is mean stress.

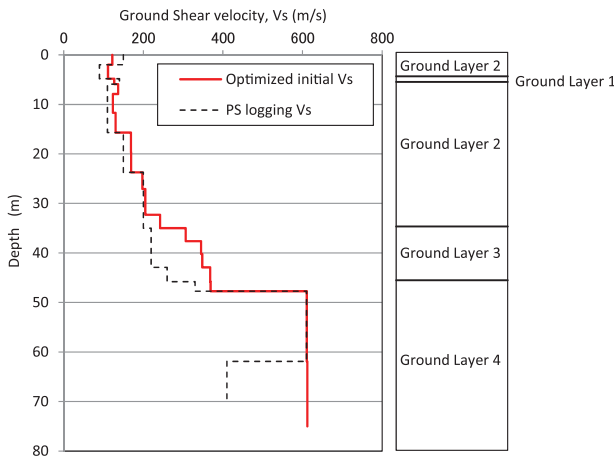


Fig. 7 Optimized initial shear wave velocity from P-S logging

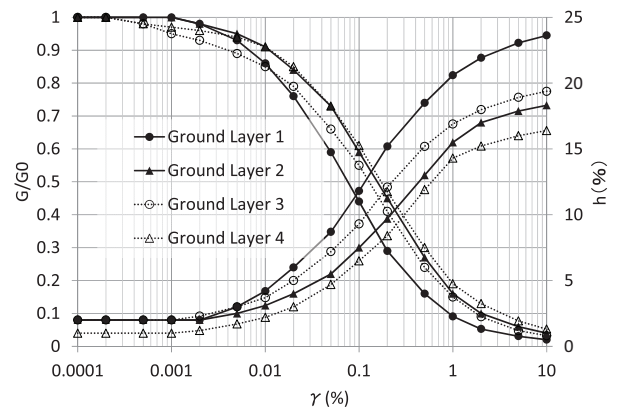


Fig. 8 Strain dependence characteristics of the soil

And Mohr-Coulomb criterion for the shear failure is expressed using stress invariants as follows

$$\sigma_m \sin \phi + (J'_2)^{\frac{1}{2}} \left(\cos \theta - \frac{1}{\sqrt{3}} \sin \theta \sin \phi \right) = c \cos \phi \quad (5)$$

where ϕ is friction angle and c is cohesion.

These criteria are shown in Fig. 9. Vertical axis is effective stress defined as follows

$$q = \sqrt{3} (J'_2)^{\frac{1}{2}} \quad (6)$$

Here, horizontal axis is mean stress. The tensile strength is evaluated correctly by taking lower strength between the two criteria.

Hayashi-Hibino model (Motojima et al., 1978) is used as a two criteria model described here in this study. Hayashi-Hibino model is nonlinear elastic model. Elastic modulus reduces to the value specified by the user when the stress reaches to the failure criteria. Hayashi-Hibino model is able to evaluate nonlinearity under the failure criteria. The index of soil nonlinearity, R , defined in Fig. 9 means the proximity to the criteria. The proximity to the tensile criterion and the proximity to Mohr-Coulomb criterion are calculated. R is taken the minimum value between the two. R becomes 0 when the stress reaches the failure criteria. Elastic moduli are reduced according to R in the following equations

$$E = R^{\frac{1}{a}} E_0 \quad (7)$$

$$0.45 - \nu = R^{\frac{1}{2a}} (0.45 - \nu_0) \quad (8)$$

where a is a parameter.

3.6 Properties of stabilized soil

The properties of the stabilized soil according to Hayashi-Hibino model are shown in Table 2. The friction angle and Poisson's ratio are set to 30 degree and 0.26, respectively. Two sets of values about cohesion, compressive strength and shear modulus are assumed. In case 1, the compressive strength of the stabilized soil was set at design standard strength, $q_0 = 1.8$ MPa. The initial shear modulus is set at 700 MPa ($\rho = 2.0$ t/m³, $V_s = 592$ m/s) and the tensile strength is set at $0.2q_0 = 360$ kPa referred to Saito and Konishi (2010). Cohesion c is set to $0.3q_0 = 540$ kPa. In case 2, the parameter set is based on the on-site compressive strength. The compressive strength of the stabilized soil was set at the average value of unconfined compression test results from 36 core samples shown in Table 3 (Yamashita et al., 2015). The tensile strength is set at $0.2q_0 = 760$ kPa. The initial shear modulus is set at 1300 MPa and cohesion c is set to $0.3q_0 = 1140$ kPa based on the compression test results. The initial vertical stress of the DMWs is set at 300 kPa which corresponds to the measured contact pressure between the raft and the DMWs (Yamashita et al., 2012). The horizontal stress is assumed to be the contact pressure multiplying the coefficient of earth pressure at rest.

The nonlinearity under the failure criteria is decided comparing the modified HD model. The model parameter is set by simulating the uniaxial compression test (Shigeno, 2015). Parameter a in equation (7) is set to 1.0, and Fig. 10 shows the G - γ

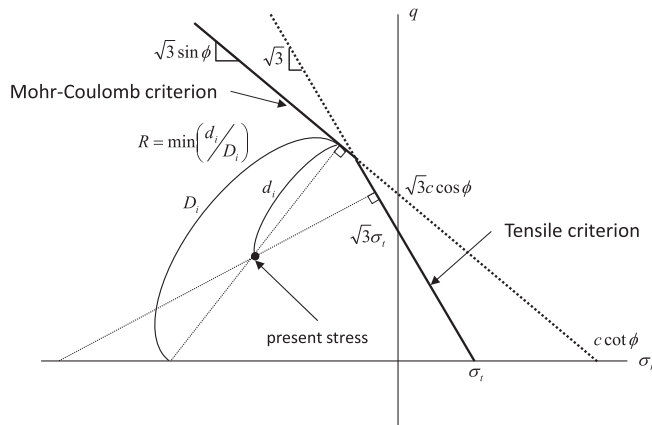


Fig. 9 Criteria of Hayashi-Hibino model

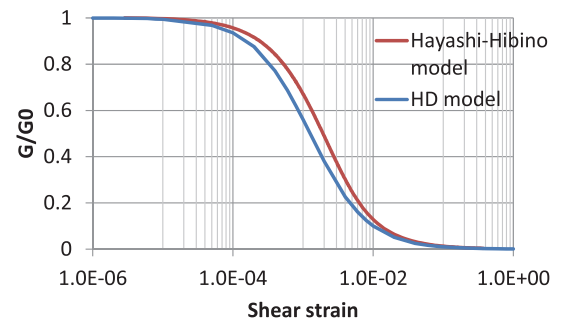


Fig. 10 Comparison of G - γ relation between Hayashi-Hibino model and HD model

Table 2 Properties of Hayashi-Hibino model for stabilized soil

	Tensile strength σ_t (kPa)	Shear modulus G_0 (MPa)	ν	Cohesion c (kPa)	Friction angle ϕ (degree)	Parameter a
case 1	360	700	0.26	540	30	1.0
case 2	760	1300	0.26	1140	30	1.0

Table 3 Unconfined compression test results of stabilized soil (age of 28 days) (Yamashita et al., 2015)

	Average (MPa)	Max. (MPa)	Min. (MPa)	COV
Unconfined compressive strength	3.81	6.79	2.64	0.25

relations based on the Hayashi-Hibino model.

4 RESULTS OF ANALYSES

4.1 Seismic simulation analysis during the 2011 earthquake

Shigeno (2015) conducted simulation analyses using the same nonlinear soil model as employed in this paper against the input ground motion during the 2011 off the Pacific coast of Tohoku Earthquake, which was categorized in a middle-scale earthquake at the site. Figure 11 shows the profiles of the peak acceleration and relative displacement to the measured point at a depth of 50 m in the EW direction. Figure 12 shows the profiles of the peak bending moment of the piles in the EW direction. The analytical values using the nonlinear soil model of acceleration and relative displacement as well as those of pile bending moment and relative displacement agreed well with the observed values. Incidentally, the analytical results using equivalent linear moduli for soil (Hamada et al., 2014) are also shown in Figs. 11 and 12, which also agreed well with the observed values. As a result, the validity of the analysis model for a middle-scale earthquake was confirmed.

4.2 Seismic response analyses under large-scale earthquakes

Three analytical cases were conducted, where tensile strength of the stabilized soil is different. In cases 1 and 2, the DMWs are modeled using Hayashi-Hibino model with the tensile strength of 360 and 760 kPa, respectively. In addition, no ground improvement is employed in case 3 where the properties of the DWMs are replaced with those of the original soil.

Figure 13 shows the profiles of the peak acceleration and relative displacement of the building and the ground in the NS direction. The peak acceleration of the ground surface is around 420 cm/s^2 under Kobe phase, 350 cm/s^2 under Hachinohe phase and 450 cm/s^2 under Northern Tokyo Bay. The peak acceleration of the top of the building is around 160 cm/s^2 under Kobe phase, 130 cm/s^2 under Hachinohe phase and 150 cm/s^2 under Northern Tokyo Bay, and less than 40% of that of the ground surface since the base isolation system functions effectively. The maximum relative surface ground displacements in

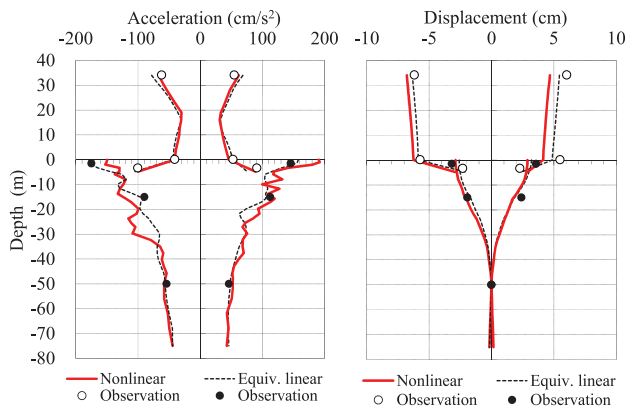


Fig. 11 Distribution of peak acceleration and relative displacement (EW direction)

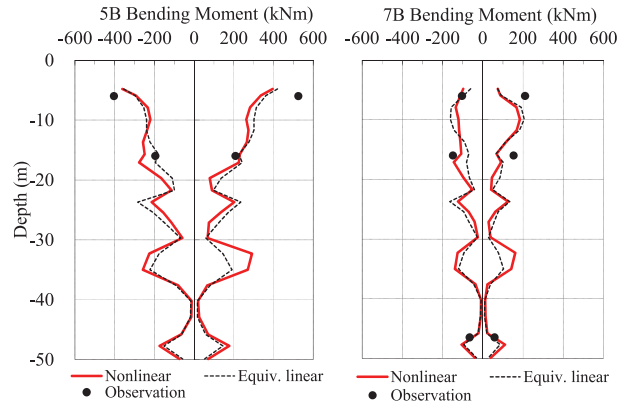
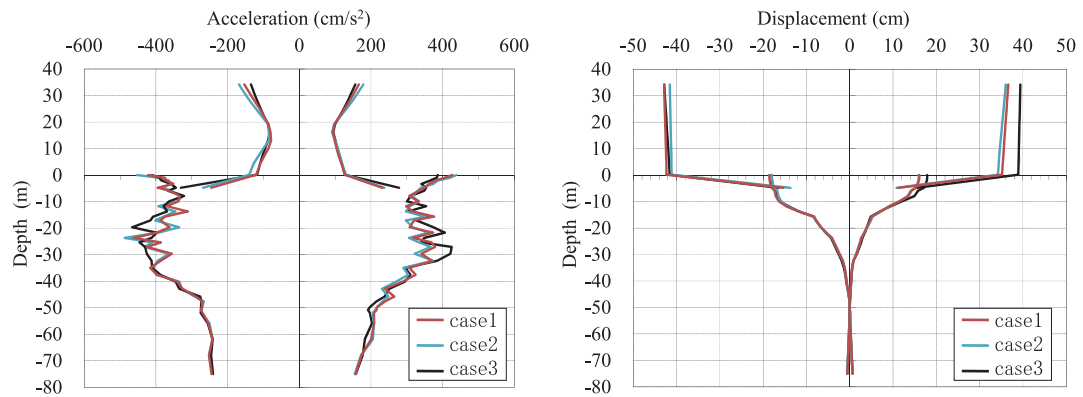


Fig. 12 Distribution of peak bending moment of the piles (EW direction)

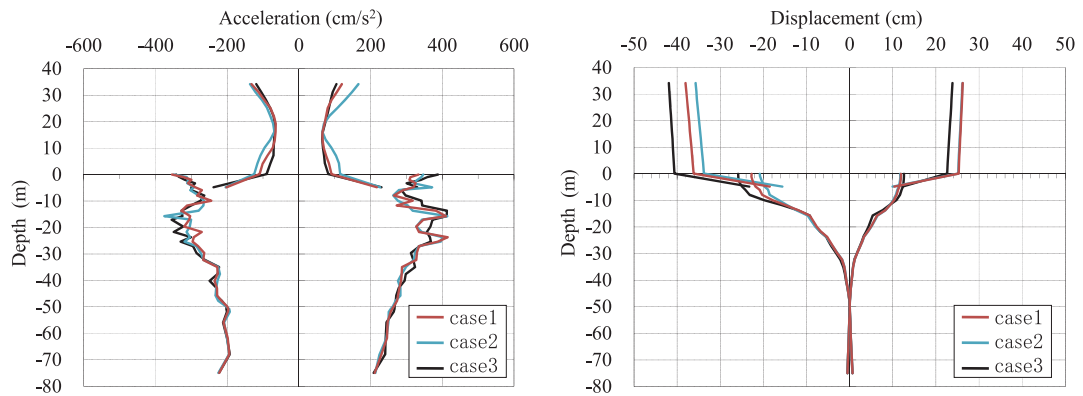
the free field are 16 to 26 cm, and the displacement under the input motion of Hachinohe phase is the largest while that of Northern Tokyo Bay is the smallest. These displacements, caused by the softening of the ground, are extremely large in comparison with those under the middle-scale earthquake shown in Fig. 11. Figure 13 also shows that the relative displacements of the raft foundation are different among the three cases, i.e., the displacements in case 3 are larger than those in cases 1 and 2. This suggests that the surface ground deformation was reduced by the DMWs.

The peak relative displacement of the building is large in Kobe phase and Hachinohe phase. The maximum gap displacements at the base-isolation layer in cases 1 and 2 are listed in Table 4. The maximum values calculated from cases 1 and 2 in Kobe phase in NS direction are 27.0 cm and 27.5 cm, respectively. Both of them are much less than design clearance of 60 cm.

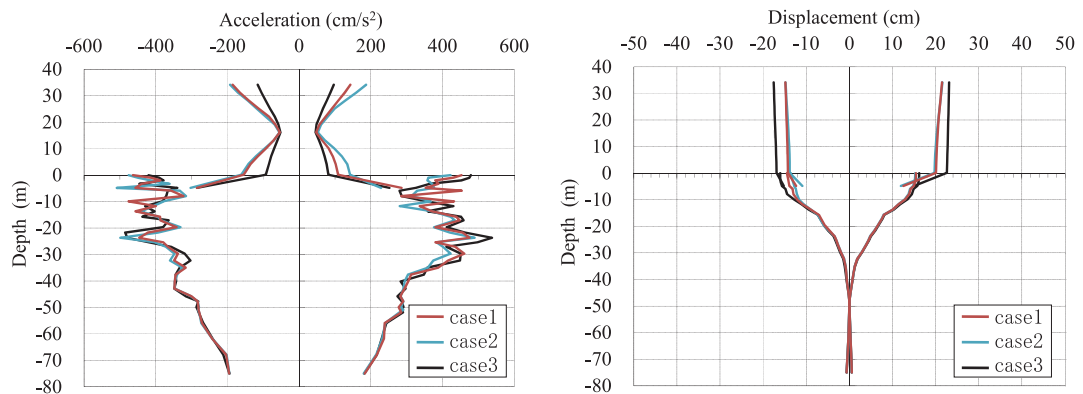
The peak displacement of the building under Northern Tokyo Bay is smaller than those under the other input motions. The



(a) Kobe phase



(b) Hachinohe phase

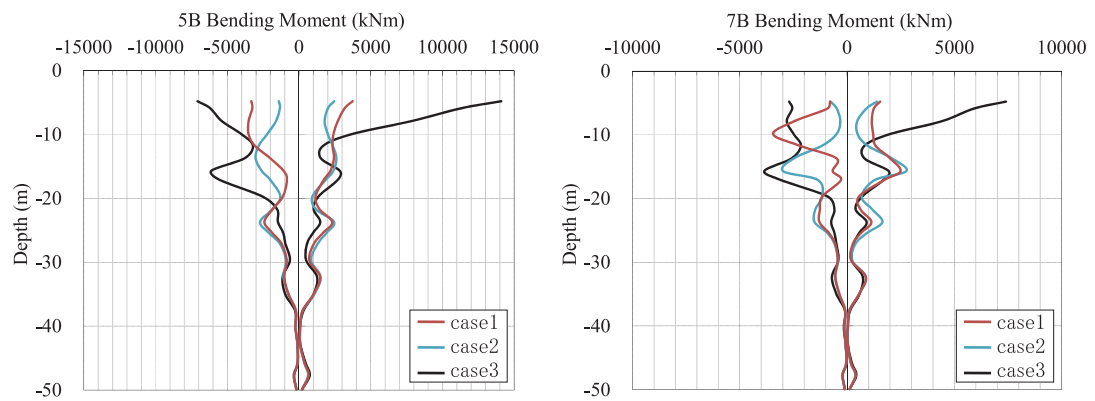


(c) Northern Tokyo Bay

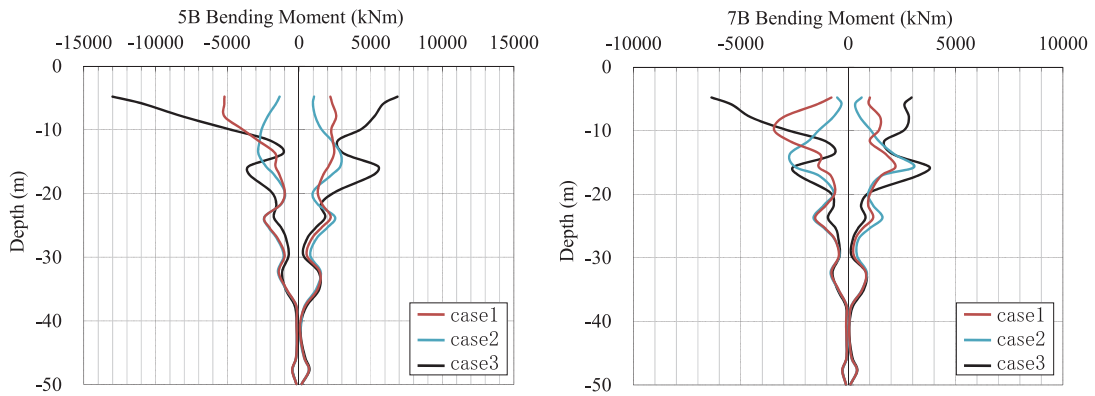
Fig. 13 Profiles of peak acceleration and relative displacement (NS direction)

Table 4 Maximum gap displacement of isolation layer (cm)

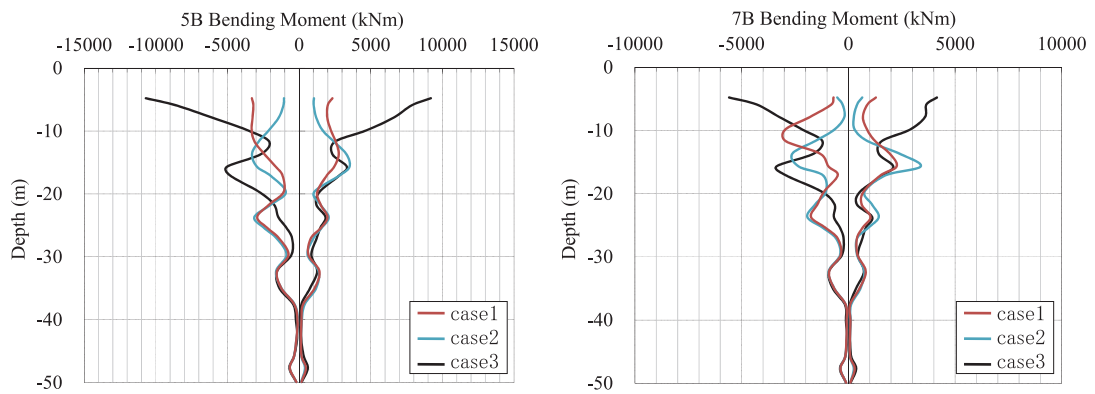
	direction	Kobe phase	Hachinohe phase	Northern Tokyo Bay
case 1	EW	22.3	16.3	7.8
	NS	27.0	17.6	7.6
case 2	EW	24.4	16.5	7.3
	NS	27.5	18.2	7.8



(a) Kobe phase



(b) Hachinohe phase



(c) Northern Tokyo Bay

Fig. 14 Profiles of peak bending moment of piles 5B and 7B (NS direction)

natural period of the model becomes 5.0 sec after the base isolation devices fully function. As shown Fig. 6, the value of acceleration response spectrum around 5.0 sec in Northern Tokyo Bay is much smaller than the others. This is the reason why this difference happens.

Figure 14 shows the profiles of the peak bending moment in Piles 5B and 7B in the NS direction. The values of the peak bending moment are significantly different among the three cases, unlike the acceleration and displacement shown in Fig. 13. The values of the peak bending moment near the pile head in case 3 (without ground improvement) are markedly larger than those in cases 1 and 2 (employing the grid-form DMWs). This suggests that the grid-form DMWs carry a significant part of the horizontal force which means the sum of inertial force of the superstructure and passive load acting on the side of the buried raft due to the relative horizontal displacement of the raft to the ground. Although the values of the bending of moment near the pile head in case 2 are smaller, those at a depth of 16 m, which corresponds to the bottom depth of the DMWs, have tendency to be larger.

Figure 15 shows the tensile failure zone in the grid-form DMWs using the maximum principal stress (note that tension is plus). The maximum tensile stress in the stabilized soil in case 1 ($\sigma_t = 360$ kPa) reached the tensile strength and the grid-form DMWs showed partial failure. In contrast, almost no damage to the DMWs occurred in case 2 ($\sigma_t = 760$ kPa). The partial failure of the DMWs may lead to the result that the values of the bending moment near the pile head in case 1 were generally larger than those in cases 2. Figure 16 shows shear failure zone in the grid-form DMWs using the closest degree to Mohr-Coulomb's criterion. Here, the failure zone means the zone with $1-R > 0.95$ (R is defined in Fig. 9). The grid-form DMWs showed partial shear failure in case 1, while no shear failure in the DMWs occurred at all in case 2.

Figure 17 shows the analytical results of NM-relationship of the piles, i.e., the relationship between the axial force and the pile head bending moment of Piles 5B and 7B, together with the interaction curves for the axial force and the bending moment of the SC pile (which was used in the top portion of 12 m). The axial force is the sum of the measured static force and the maximum and minimum dynamical increment force in the analysis, and the bending moment is the maximum value along the SC pile. Here, the ultimate criterion is defined when the unit stress at the edge of the concrete reaches the compressive strength

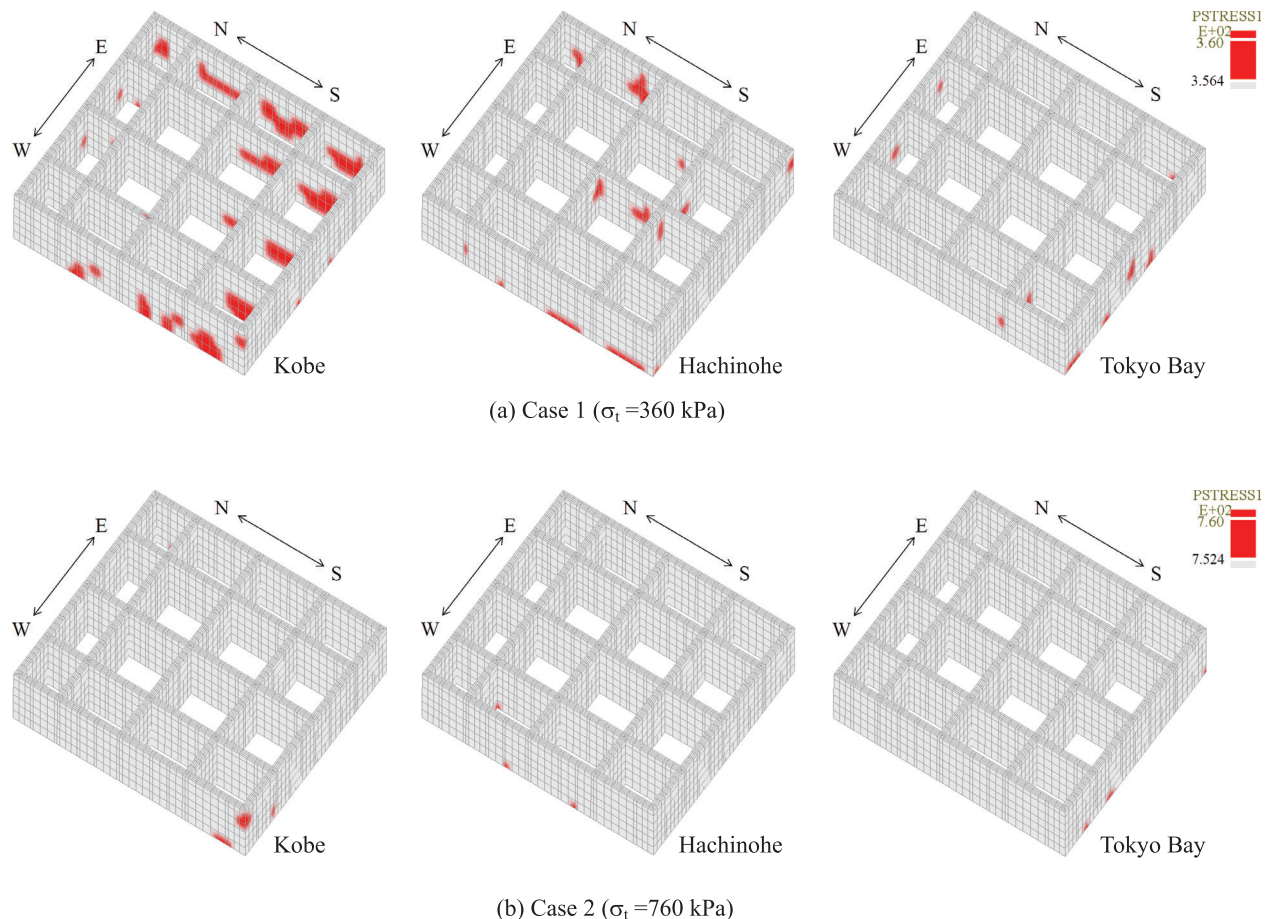


Fig. 15 Tensile failure zone in grid-form DMWs

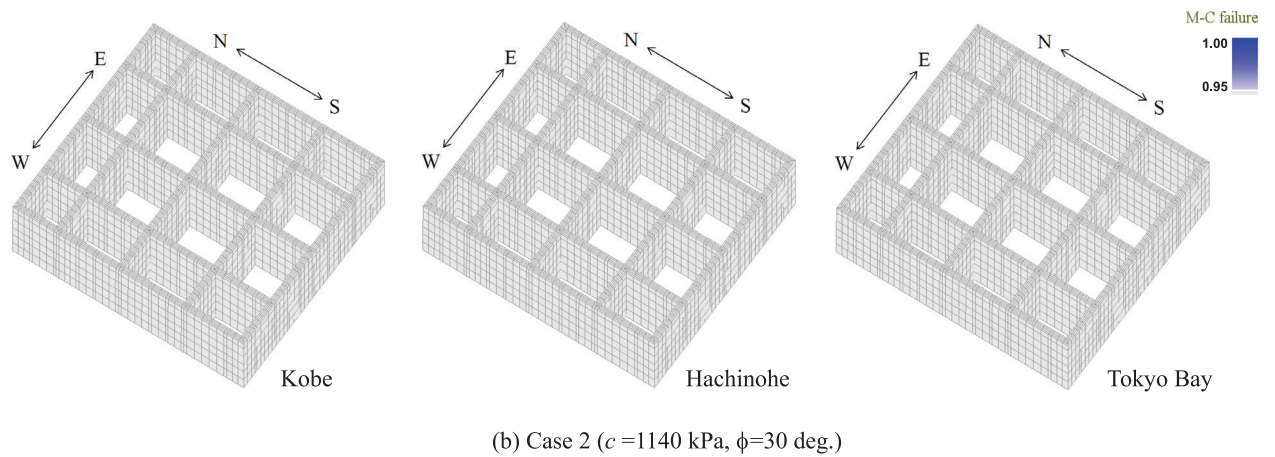
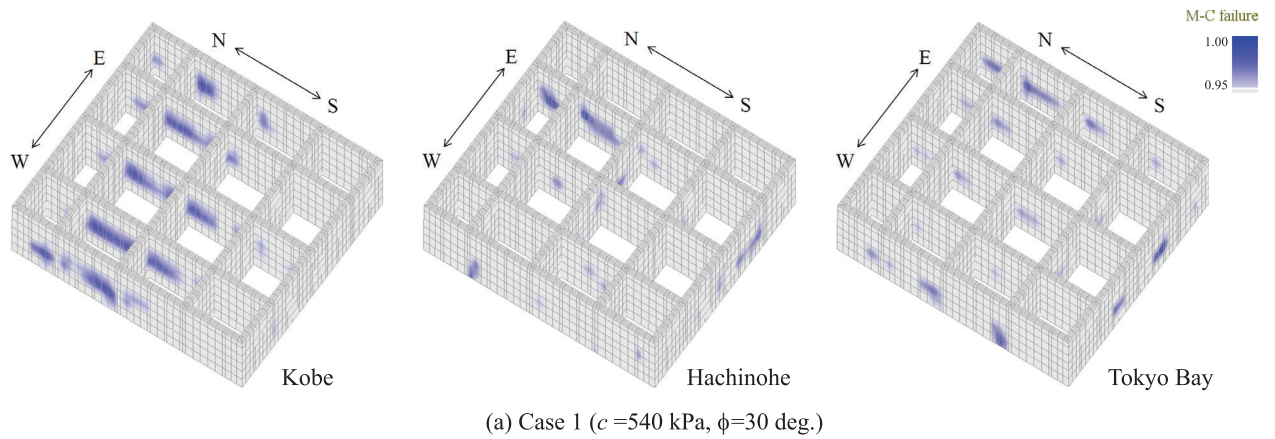


Fig. 16 Shear failure zone in grid-form DMWs

of 105 N/mm^2 in compression and the compressive strain at the edge reaches 5000 micro strain. The allowable criterion for middle-scale earthquakes is defined when the unit stress at the edge of the steel pipe reaches 325 N/mm^2 in tension and/or the unit stress at the edge of the concrete reaches 60 N/mm^2 (105 N/mm^2 divided by a safety factor, 1.75) in compression.

The numerical results indicate that the maximum bending moments in cases 1 and 2 are below or close to the allowable criterion, and significantly below the ultimate criterion, whereas those in case 3 are markedly large and beyond or close to the ultimate criterion.

Figures 15 to 17 showed that the grid-form DMWs are effective in reducing the pile bending moments to an acceptable level, as well as preventing soil liquefaction. Although the pile bending moments in case 1 ($\sigma_t = 360 \text{ kPa}$) are somewhat larger than those in case 2 ($\sigma_t = 760 \text{ kPa}$), the grid-form DMWs are effective in reducing the pile bending moments even if the induced stress in the stabilized soil reaches partially the tensile and shear strength during the large earthquakes. This may be attributed to that the ground displacements near the surface in case 1 are larger than those in case 2 but clearly smaller than those in case 3 (without ground improvement) as can be seen in Fig. 13.

Although partial damage to the grid-form DMWs is not allowed in current allowable stress design method, Namikawa et al (2007) have pointed out that the grid-form DMWs can be designed more rationally by the performance-based design method in which a partial failure of the DMWs is accepted. The performance-based design requires an accurate evaluation of the effects of partial damage on the behavior of piles surrounded by the DMWs. The numerical results suggest that the nonlinear 3D FE analysis employed in this study can provide adequate solutions for the performance-based seismic design of piled rafts with the grid-form DMWs.

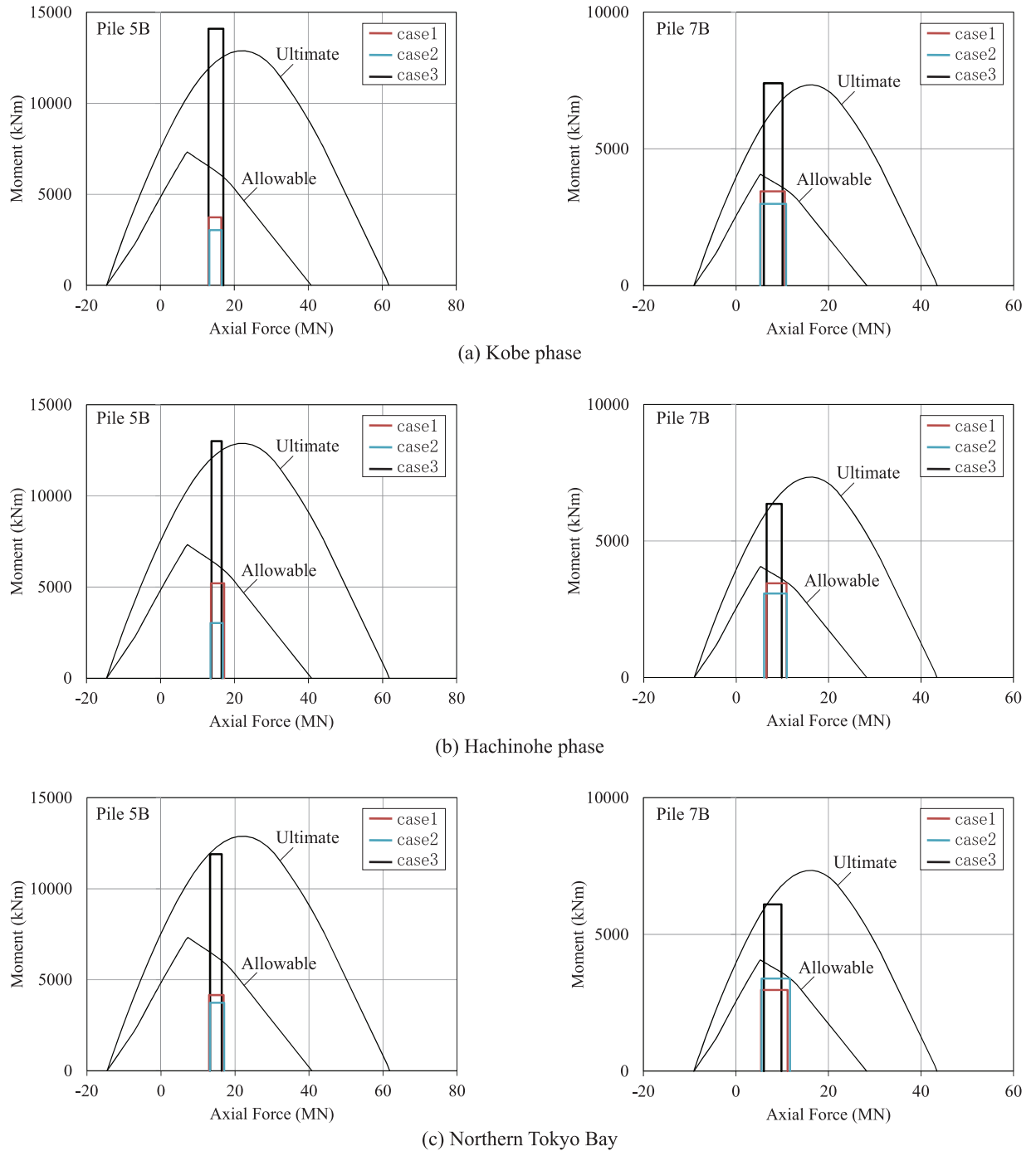


Fig. 17 NM-relationship of SC piles, and calculated values (NS direction)

5 CONCLUSIONS

Nonlinear seismic response analyses under large-scale earthquakes using a detailed 3D FE ground and structure interaction model were conducted. A multi-hardening model is used as the constitutive model of the soil which incorporates the elasto-plastic model into the Yoshida model. As the input ground motions which are defined by about 500 years recurrence interval, two Japanese notification waves of Kobe and Hachinohe phases as well as Northern Tokyo Bay earthquake which was simulatively generated by the Central Disaster Management Council of Japan were chosen as maximum consideration earthquakes. The ground conditions were set in three cases; two cases employing the DMWs of different strength of the stabilized soil and a case without ground improvement.

Based on the numerical results, the maximum surface ground displacements in the free field were very large, 19 to 26 cm,

and the bending moments of piles in case 3 (without ground improvement) were markedly large and beyond or close to the ultimate criterion of the NM relation of SC pile, while those in cases 1 and 2 (employing the grid-form DMWs) were considerably below the ultimate criterion. This arises because the grid-form DMWs carry a significant part of the horizontal force. Consequently, it was found that the grid-form DMWs are quite effective in reducing the sectional force of piles to an acceptable level even if the induced stress in the DMWs partially reaches the tensile and shear strength during the large earthquakes. In other words, the sectional force of the piles would be affected significantly by the strength of the stabilized soil. The numerical results also suggest that the nonlinear 3D FE analysis employed in this study can provide adequate solutions for the performance-based seismic design of piled rafts with the grid-form DMWs.

ACKNOWLEDGMENTS

The results were obtained by using the K computer at the RIKEN Advanced Institute for Computational Science (Proposal number hp150063) and TSUBAME2.5 supercomputer in the Tokyo Institute of Technology supported by the MEXT Project for Creation of Research Platforms and Sharing of Advanced Research Infrastructure. And also this work was supported by the JSPS KAKENHI Grant (No. 26289197).

REFERENCES

- Hamada, J., Tanikawa, T., Onimaru, S. and Yamashita, K. (2012): Seismic observations on piled raft foundation with ground improvement supporting a base-isolated building, Proc. of the 15thWCEE.
- Hamada, J., Shigeno, Y., Onimaru, S., Tanikawa, T., Nakamura, N., Yamashita, K. (2014): Numerical analysis on seismic response of piled raft foundation with ground improvement based on seismic observation records, Proc. of the 14th IACMAG.
- Ishihara, K., Yoshida, N. and Tsujino, S. (1985): Modeling of stress-strain relations of soils in cyclic loading, Proc. of the 5th International Conference for Numerical Method in Geomechanics, Nagoya, Vol.1, 115-143.
- Motojima, M., Hibino S. and Hayashi, M. (1978): Development of computer program for stability analysis of excavation, Central Research Institute of Electric Power Industry Report No 377012 (in Japanese).
- Namikawa, T., Koseki, J. and Suzuki, Y. (2007): Finite element analysis of lattice-shaped ground improvement by cement-mixing for liquefaction mitigation, Soils & Foundations, Vol.47, No.3, 559-576.
- Onimaru, S., Hamada, J., Nakamura, N. and Yamashita, K. (2012): Dynamic soil-structure interaction of a building supported by piled raft and ground improvement during the 2011 Tohoku Earthquake, Proc. of the 15thWCEE.
- Saito, S. and Konishi, K. (2010): Proceeding of the 9th national symposium on ground improvement, Elastic constant for design of cement-improved soil, 287-292 (in Japanese).
- Shigeno, Y., Hamada, J. and Nakamura, N. (2014): Hybrid parallelization of earthquake response analysis using K computer, Proc. of the 14th IACMAG.
- Shigeno, Y. (2015): Nonlinear analysis of seismic response of a base isolated building on a piled raft foundation with grid-form ground improvement, Proc. of the 15th Asian Regional Conference on Soil Mechanics and Geotechnical Engineering.
- Shiomi, T., Yoshizawa, M., Onimaru, S. and Tsukuni, S. (1998): Development of structural analysis system considering non-linear behaviors of soil and structure, Takenaka Technical Research Report, No.54, 1-8 (in Japanese).
- Shiomi, T. and Fujiwara, Y. (2014): Liquefaction analysis of Urayasu-site by the multi-hardening model, Proc. of the special symposium of JGS -Overcoming the Great East Japan Earthquake-, 141-145 (in Japanese).
- Yamashita, K., Hamada, J. and Yamada, T. (2011): Field measurements on piled rafts with grid-form deep mixing walls on soft ground, Geotechnical Engineering Journal of the SEAGS & AGSSEA, Vol.42, No.2, 1-10.
- Yamashita, K., Hamada, J., Onimaru, S. and Higashino, M. (2012): Seismic behavior of piled raft with ground improvement supporting a base-isolated building on soft ground in Tokyo, Soils & Foundations, Special Issue on Geotechnical Aspects of the 2011 off the Pacific Coast of Tohoku Earthquake, Vol.52, No.5, 1000-1015.
- Yamashita, K., Tanikawa, T., Shigeno, Y. and Hamada, J. (2015): Vertical load sharing of piled raft with grid-form deep mixing walls, Proc. of Conference on Deep Mixing 2015, 437-446.
- Yoshida, N. and Tsujino, S. (1993): A simplified practical stress-strain model for the multi-dimensional analysis under repeated loading, The 28th Japan national conference on soil mechanics and foundation engineering, pp.1221-1224 (in Japanese).

Corrections

Erratum for “Numerical Analyses of a Piled Raft Foundation with Grid-Form DMWs under Large-Scale Earthquakes”
“格子状地盤改良を併用したパイルド・ラフト基礎のレベル2 地震に対する解析的検討”

Yoshimasa Shigeno 重野喜政 Junji Hamada 濱田純次 Naohiro Nakamura 中村尚弘 Kiyoshi Yamashita 山下清

In the original paper, Figs. 15 and 16 were incorrectly published. The correct figures appear below. The publisher would like to apologize for any inconvenience caused.

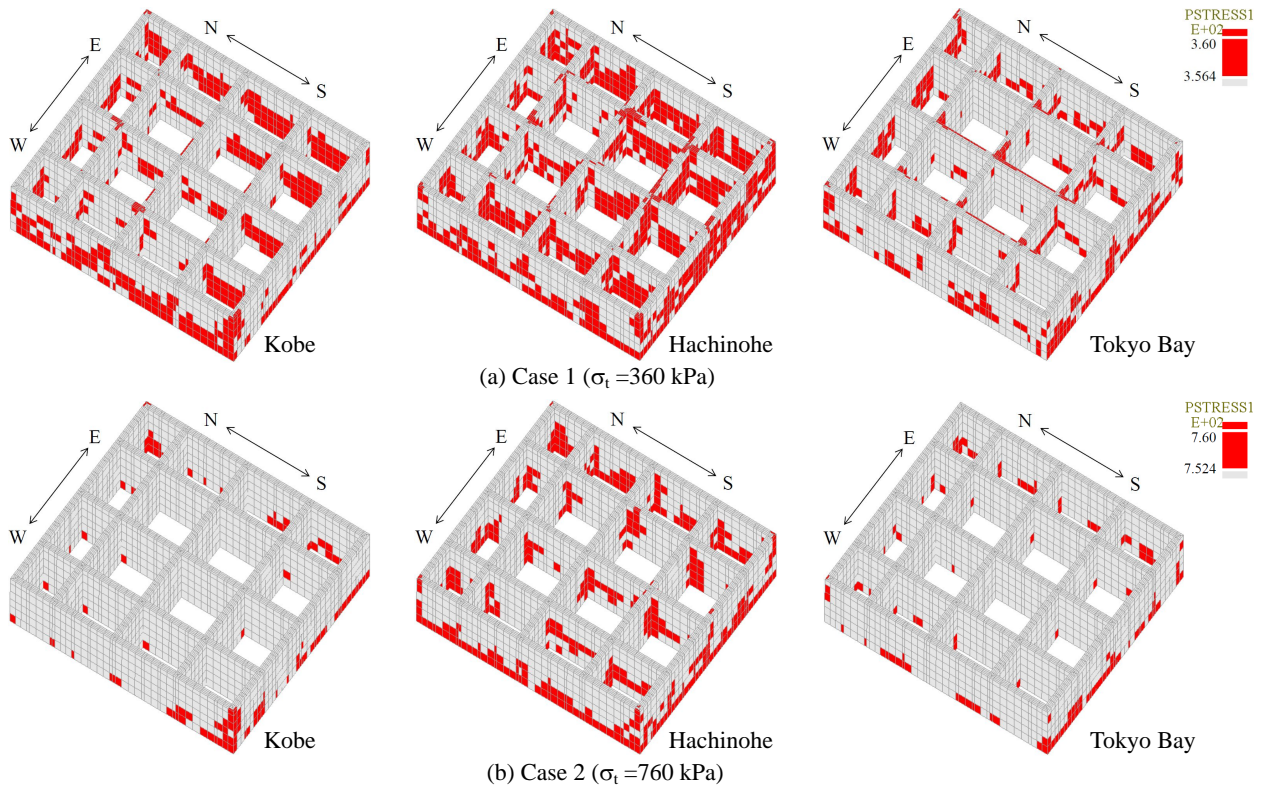


Fig. 15 Tensile failure zone in grid-form DMWs

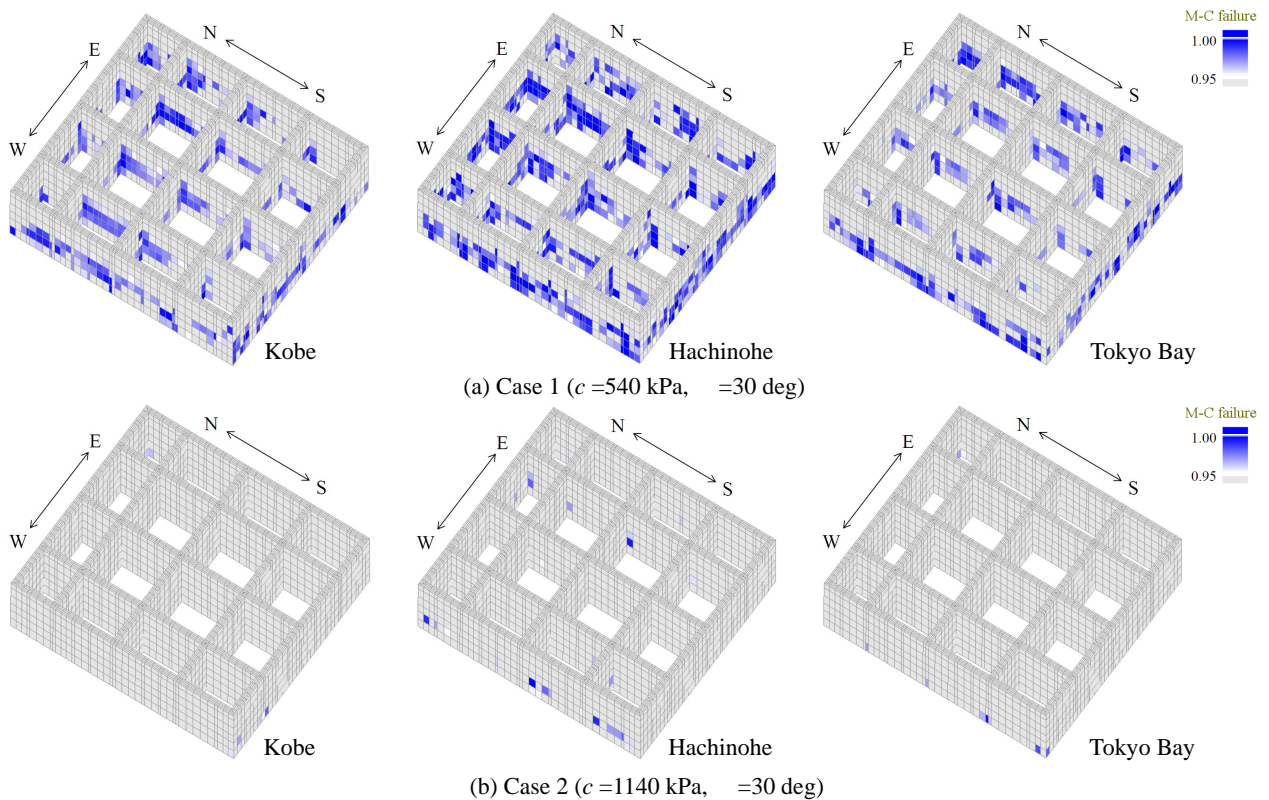


Fig. 16 Shear failure zone in grid-form DMWs